Journal of Cerebral Blood Flow & Metabolism (2012) 32, 278–290

www.jcbfm.com

The pathologic cascade of cerebrovascular lesions in SHRSP: is erythrocyte accumulation an early phase?

Stefanie Schreiber[1], Celine Z Bueche[1], Cornelia Garz[1], Siegfried Kropf[2], Frank Angenstein[1,3,4], Juergen Goldschmidt[1,4], Jens Neumann[1], Hans-Jochen Heinze[1,3,4], Michael Goertler[1], Klaus G Reymann[3,4] and Holger Braun[3,4]

[1]*Klinik für Neurologie, Otto-von-Guericke Universität, Magdeburg, Germany;* [2]*Institut für Biometrie und Medizinische Informatik, Otto-von-Guericke Universität, Magdeburg, Germany;* [3]*Deutsches Zentrum für Neurodegenerative Erkrankungen, Magdeburg, Germany;* [4]*Leibniz Institut für Neurobiologie, Magdeburg, Germany*

Cerebral small vessel disease (CSVD) is associated with vessel wall changes, microbleeds, blood–brain barrier (BBB) disturbances, and reduced cerebral blood flow (CBF). As spontaneously hypertensive stroke-prone rats (SHRSP) may be a valid model of some aspects of human CSVD, we aimed to identify whether those changes occur in definite temporal stages and whether there is an initial phenomenon beyond those common vascular alterations. Groups of 51 SHRSP were examined simultaneously by histologic (Hematoxylin–Eosin, IgG-Immunohistochemistry, vessel diameter measurement) and imaging methods (Magnetic Resonance Imaging, 201-Thallium-Diethyldithiocarbamate/99m-Technetium-HMPAO Single Photon Emission Computed Tomography conducted as pilot study) at different stages of age. Vascular pathology in SHRSP proceeds in definite stages, whereas an age-dependent accumulation of erythrocytes in capillaries and arterioles represents the homogeneous initial step of the disease. Erythrocyte accumulations are followed by BBB disturbances and microbleeds, both also increasing with age. Microthromboses, tissue infarctions with CBF reduction, and disturbed potassium uptake represent the final stage of vascular pathology in SHRSP. Erythrocyte accumulations—we parsimoniously interpreted as stases—without cerebral tissue damage represent the first step of vascular pathology in SHRSP. If that initial phenomenon could be identified in patients, these erythrocyte accumulations might be a promising target for implementing prophylactic and therapeutic strategies in human CSVD.
Journal of Cerebral Blood Flow & Metabolism (2012) **32,** 278–290; doi:10.1038/jcbfm.2011.122; published online 31 August 2011

Keywords: animal models; blood–brain barrier; microcirculation; SPECT; white matter disease

Introduction

Human cerebral small vessel disease (CSVD), one of the leading causes of cerebral ischemia (Amarenco *et al*, 2009), is not only associated with stroke-like symptoms but also with cognitive impairments that occur in vascular dementia. As human CSVD substantially contributes to late-life brain atrophy and dementia in a population with increasing number of older individuals (Fotuhi *et al*, 2009), studies of the natural pathophysiology of CSVD are of pivotal importance.

Human CSVD and associated lacunar strokes are believed to be caused by degenerative vessel wall alterations of the small arteries and arterioles. These changes include endothelial proliferation, hyaline concentric vessel wall thickening, and small vessel occlusions (Grinberg and Thal, 2010). Additional disturbances of the blood–brain barrier (BBB) and associated (vasogenic) edema are indicated by plasma protein leakage (Nag *et al*, 2009; Michalski *et al*, 2010). Besides these changes, microbleeds have been described to occur frequently in human CSVD (Gouw *et al*, 2010).

We aimed to identify whether these pathologic changes associated with human CSVD proceed in definite stages and whether there is an initial phenomenon beyond the common vascular

Correspondence: Dr S Schreiber, Department of Neurology, Otto-von-Guericke University, Leipziger Strasse 44, 39120 Magdeburg, Germany.
E-mail: stefanie.schreiber@med.ovgu.de
JG and KGR are supported by the Federal Ministry of Education and Research Project: 'Präklinische Evaluierung von Metallchelatkomplexen als Tracer zur Untersuchung des zerebralen Ionen-Metabolismus.' FKZ: 01 SF 0718.
Received 7 February 2011; revised 22 May 2011; accepted 14 June 2011; published online 31 August 2011

alterations. To implement prophylactic and therapeutic strategies in patients with CSVD, it is of utmost importance to define that initial pathologic vascular event, if existing as a single phenomenon.

To identify definite stages and the possible initiation phenomenon of CSVD, we examined the vascular pathology of spontaneously hypertensive stroke-prone rats (SHRSP) at different stages of age. These rats provide an animal model that is accepted as a potentially relevant model to the study of CSVD (Hainsworth and Markus, 2008). Therefore, histologic data from SHRSP at different ages were combined here with Magnetic Resonance Imaging (MRI) and Single Photon Emission Computed Tomography (SPECT) data to elucidate cerebrovascular changes in SHRSP.

Furthermore, BBB disturbances were illustrated by leakage of IgG into the vessel wall. The vasogenic edema and tissue infarctions were detected by MRI; cerebral blood flow (CBF) was measured using 99m-Technetium-HMPAO (99m-Tc-HMPAO) as a tracer for performing SPECT. In addition, to evaluate possible disturbances of potassium uptake, 201-Thallium-Diethyldithiocarbamate (201-Tl-DDC) SPECT was performed.

Our results show that the vascular pathology in SHRSP is initiated by an accumulation of erythrocytes in capillary and arteriolar segments. This initial step is not accompanied by BBB disturbances, microbleeds, or tissue infarctions, representing the subsequent stages in the pathologic cascade of the cerebral vascular pathology.

Materials and methods

Animals

Animal procedures were conducted after obtaining the approval of the Animal Care Committee of Sachsen Anhalt (reference number of license for animal testing 42502-2-943, July 2009, Magdeburg, Sachsen-Anhalt). Animals were housed with a natural light–dark cycle and allowed to access water and food *ad libitum*.

Groups of two to 11 animals of a total of 51 male SHRSP (Charles River Laboratories International Inc., Wilmington, MA, USA) were investigated histologically at ages between 12 and 42 weeks (12 to 14 weeks—$n = 11$, 16 to 18 weeks—$n = 6$, 24 to 26 weeks—$n = 2$, 28 weeks—$n = 8$, 32 weeks—$n = 8$, 34 to 36 weeks—$n = 9$, 40 to 42 weeks—$n = 4$). Animals were monitored daily for alterations in their neurologic status (such as decreased spontaneous activity, coordination failure, falling to one side, hunched posture) and twice a week for decreased body weight. In all, 12 Wistar rats with corresponding ages served as a control group (12 weeks—$n = 2$, 18 weeks—$n = 4$, 26 weeks—$n = 2$, 32 weeks—$n = 2$, 65 weeks—$n = 2$).

Histology

Rats were transcardially perfused with 120 mL phosphate-buffered saline to remove blood completely, followed by 120 mL of 4% paraformaldehyde within 4 minutes. Their brains were removed, perfused with 4% paraformaldehyde for 48 hours, placed for cryo-protection into 30% sacharose for 6 days, and frozen in methylbutane at -80°C. Coronal slices of the whole brain were prepared using a cryotoma (Leica, Nussloch, Germany). Staining with Hematoxylin–Eosin (HE) and Congo Red were performed. From the frontal to the occipital pole, there were 10 to 11 sectional planes per animal, whereas the first sectional plane was a remote 930 μm from the frontal pole. The distance between each sectional plane was 1 mm. Three slices per brain sectional plane were stained; thus, 30 to 33 slices per animal were stained with HE and Congo Red. Congo Red was applied to detect a possible Cerebral Amyloid Angiopathy (CAA). These slices were subjected to light microscopic examinations (Leica DMR), which included the use of polarized light to detect the presence of apple-green birefringence in the small vessel walls.

For all SHRSP and the whole control group, the occurrence (existent or not existent) of vessels with accumulated erythrocytes and the occurrence of microbleeds (existent or not existent) were assessed within the hippocampus, the basal ganglia, the corpus callosum, and the cortex within all sectional areas of the HE slices at all stages of age. In both animal groups, the luminal diameter of those vessels showing accumulated erythrocytes was measured in at least three HE slices per animal. The capillary diameter ranged from 5 to 22 μm (Ley *et al*, 1986), and the arteriolar diameter ranged from 20 to 65 μm (Yang *et al*, 1991).

Immunohistochemistry

Repeated washing of the sections in phosphate-buffered saline and blocking with 0.1 mol/L phosphate-buffered saline, 0.5% TritonX, and 10% donkey serum (Sigma, St Louis, MO, USA) were followed by staining with anti-solanum tuberosum lectin (STL) antibody overnight at 4°C in phosphate-buffered saline containing 5% donkey serum. Slices were washed anew before application of anti-IgG-Cy3 for 2 hours at room temperature and subsequent DAPI staining (20 minutes, room temperature). As a control, first antibodies were omitted during immunohistochemistry staining. After increasing concentrations of alcohol, slices were mounted by Histomount.

Solanum tuberosum lectin (Vector Laboratories, Burlingame, CA, USA) is a fluorescein-labeled potato lectin containing $\sim$50% carbohydrate, mainly composed of arabinose and galactose (Vector Laboratories (Van Damme *et al*, 2004)). Solanum tuberosum lectin binds on glycoproteins on the surface of endothelial cells and microglia (Michalski *et al*, 2010) and was used for vessel staining in a dilution of 1:500. Anti-laminin antibody (Abcam, Cambridge Science Park, Cambridge, UK) detects laminin, which is a component of the basal membrane and was used in a dilution of 1:500. CY3-donkey anti-rat IgG was used for detection of IgG and Cy5-donkey anti-rabbit IgG as secondary antibody for anti-laminin in a dilution of 1:500.

In 9 SHRSP of different ages (18 weeks—$n = 1$, 24 weeks—$n = 1$, 28 weeks—$n = 2$, 32 weeks—$n = 2$, 34 weeks—$n = 1$, 36 weeks—$n = 2$), we identified the number

of immunohistochemically stained vessels in the hippocampus, the basal ganglia, the corpus callosum, and the cortex. Three slices per brain region were investigated. We determined the density of STL- and IgG-positive vessels by counting them within at least 10 counting boxes per animal and region. The ratios of IgG- and STL-positive vessels were than calculated for each counted area.

Statistics

We evaluated the presence of vessels with accumulated erythrocytes and microbleeds (existent or not existent) within the 4 different brain regions of all HE slices (30 to 33) per animal. All stages of age were investigated. To compare the SHRSP and the control group, Fisher's exact probability test for 2×2 contingency tables was used. Using the two-sided linear-by-linear association χ^2 test (exact version), the occurrence of vessels with accumulated erythrocytes and microbleeds at different ages was evaluated in the group of SHRSP and in the Wistar group.

We used a mixed model analysis with age as fixed and the animal number as random effects and a Bonferroni adjustment to calculate a possible change in the small vessel diameter with age in the SHRSP group. We performed a *t*-test to compare the diameters of small vessels between the control group and SHRSP.

Using a mixed model analysis with the different brain regions as fixed and age as random effects, we investigated the immunohistochemistry data of the SHRSP group. Owing to the unsymmetrical spread of ratios, a linear regression analysis was carried out after transformation of the data using a square root function, resulting in a second-order regression function after the inverse transformation. Using a Bonferroni adjustment, we performed a pairwise comparison between the different brain regions. *P*-values < 0.05 were deemed to be statistically significant.

Imaging

Magnetic Resonance Imaging was performed in groups of 15 SHRSP every second week from the 12th to the 42nd week of age. If one of the MR Images showed abnormalities, that animal subsequently underwent 201-Tl-DDC SPECT. One 42-week-old rat with a progressive weight loss of 38 g within 4 weeks and decreased spontaneous activity was examined simultaneously with 201-TI-DDC SPECT and 99m-Tc-HMPAO SPECT. Subsequently, after SPECT was performed, rats were perfused to investigate the corresponding histology.

Magnetic Resonance Imaging

Animals were anesthetized with 1.0% to 1.5% isoflurane (in 50:50 N_2O:O_2; volume ratio) and secured using a head holder with a bite bar to reduce motion artifacts. Magnetic Resonance Imaging experiments were performed on a Bruker Biospec 47/20 scanner at 4.7 T (Bruker, Bruker BioSpin MRI GmbH, Rudolf-Plank-Strasse, Ettlingen, Germany; free-bore diameter of 20 cm) equipped with a BGA 09 (400 mT/m) gradient system. A 50-mm Litzcage small animal imaging system (DotyScientific Inc., Columbus, SC, USA) was used for radiofrequency excitation and signal reception. T_2 weighted images with coronal, axial, and sagittal slice orientation were measured using a RARE (rapid-acquisition relaxation-enhanced) imaging sequence (Hennig *et al*, 1986) with the following parameters: repetition time 4,000 milliseconds; echo time 15 milliseconds; slice thickness 0.8 mm; distance between slices 0.8 mm; field of view $40 \times 40\,mm^2$; matrix 256×256 (resulting in a nominal in-plane resolution of 156 μm); RARE factor 8; number of averages 6. Time of Flight Angiography was performed to exclude an occlusion of the large arteries of the skull base.

201-Thallium-Diethyldithiocarbamate and 99m-Technetium-HMPAO SPECT Imaging

Single Photon Emission Computed Tomography Imaging was performed as a pilot study in three rats (2×32 weeks of age, 1×42 weeks of age). Two different tracers were used: 201-Tl-DDC and 99m-Tc-HMPAO. TlDDC is a lipophilic chelate complex that crosses the BBB (de Bruine *et al*, 1985). It has recently been shown that after crossing the BBB, the K^+-analog thallium (Tl^+) is released from TlDDC (Goldschmidt *et al*, 2010). When animals are intravenously injected with TlDDC, neurons in the central nervous system take up Tl^+ in an activity-dependent manner (Goldschmidt *et al*, 2010). TlDDC can thus be used for imaging central nervous system K^+ uptake.

201-Thallium-Diethyldithiocarbamate as used for SPECT Imaging was prepared in a similar manner as described by de Bruine *et al* (1985). A 4% NaDDC solution was prepared by adding 1 g NaDDC trihydrate (Sigma) to 25 mL of a 0.9% NaCl solution. This solution was diluted 1:10 in a 201-Tl solution to yield a 0.4% DDC (sodium diethyldithiocarbamate trihydrate) concentration in the injection solution. The 201-Tl solution contained 100 MBq 201-Tl in 0.9% NaCl in volumes of 0.7 to 0.9 mL. Injections were made into the femoral vein under isoflurane anesthesia 5 to 10 minutes after mixing 201-Tl with DDC.

99m-Technetium-HMPAO was used for imaging CBF (Neirinckx *et al*, 1987). The tracer was prepared from commercial kit preparations (Ceretec, GE Healthcare, Buchler, Braunschweig, Germany). Injections were made into the femoral vein under isoflurane anesthesia directly after preparing the tracer. Therefore, no stabilizer for 99m-Tc-HMPAO was used.

During an initial study, two rats were injected each with 100 MBq 201-Tl-DDC. In one animal, a dual isotope study was performed. This rat was injected with both tracers: 201-Tl-DDC and 99m-Tc-HMPAO. In all, 50 MBq of each tracer was injected.

Single Photon Emission Computed Tomography/Computed Tomography (CT) Imaging was performed using a four-head NanoSPECT/CT scanner. Animals were scanned under gas anesthesia (1.0% to 1.5% isoflurane in 2:1 O_2:N_2O volume ratio). Animals were scanned with nine-pinhole apertures with 2.5- or 1.5-mm pinhole diameters. Overall, 24 projections were scanned during a scan time of two hours. Axial field of view was 49 mm. Photopeaks were

set to the default values of the NanoSPECT/CT. For 201-Tl, peaks were set to 72 keV ±10% and 167 keV ±7.5%. For the 99m-Tc/201-Tl, dual isotope study peaks were set to 140 keV ±5% for 99m-Tc and 72 keV ±5% and 167 keV ±2.5% for 201-Tl.

Pinholes of 2.5 mm were used in the initial 201-Tl-DDC study, 1.5-mm pinholes were used in the dual isotope study. Images from measurements made with the 2.5-mm pinhole aperture were reconstructed at fine reconstruction settings with voxel output dimensions of 400 μm corresponding to about six times the actual spatial resolution at the given pinhole diameter. Images from measurements made with the 1.5-mm pinhole aperture were reconstructed with standard reconstruction settings at voxel output dimensions of 500 μm corresponding to about three times the spatial resolution at the given pinhole diameter. Data were displayed using scales ranging from 0 to 32,000 with 32,000 representing the highest count rate for a voxel within a data set.

Computed Tomography Scans (55 kV, 360 projections, 500 milliseconds per projection) with 200 μm resolution were performed from the same field of view as SPECT scans and coregistered with SPECT scans. Both CT and SPECT Images were reconstructed using the manufacturer's software (InVivoScope, Bioscan Inc., Washington DC, USA) and analyzed using the OsiriX-DICOM viewer for Mac OS X (Apple, Cupertino, CA, USA). Single Photon Emission Computed Tomography/CT Images were fused. For the figures, SPECT/CT Images were displayed with 50% transparency of SPECT Images.

Results

During a time span of 4 weeks, one 42-week-old SHRSP had a progressive loss of body weight from 356 to 318 g. This weight reduction was accompanied by a decrease of spontaneous activity.

The remaining animals had an average body weight of ~250 g at an age of 12 weeks, and ~400 g at 36 weeks. From the 26th week, their weight remained almost stable, with no relevant increase during the remaining 16 weeks. None of these animals had obvious neurologic symptoms. One rat died during catheterization, and two died spontaneously for reasons that remain unclear.

Accumulation of Erythrocytes

We examined the brain histology of animal groups by HE staining starting from 12 and ending at 42 weeks. In young SHRSP (12 weeks), we found no noticeable peculiarities except that few vessels contained apparently grouped or even clumped erythrocytes (Figure 1), occurring in the basal ganglia, the hippocampus, cortical regions, and the corpus callosum. We referred to these erythrocyte accumulations parsimoniously as stases, which we occasionally also detected in control animals, but with a significant lower frequency compared with SHRSP (any of the brain regions odds ratio (OR) = 17.6, $P = 0.0001$; hippocampus OR = 24.2, $P = 0.0002$; basal ganglia OR = 20.1, $P = 0.0007$; corpus callosum OR = 2.8, $P = 0.1823$; cortex OR = 9.2, $P = 0.0585$). Thus, compared with the SHRSP group, the percentage (3 of 12 animals, 25%) of control animals with erythrocyte accumulations was relatively low and, even if present, erythrocyte accumulations in a control brain could be hardly detected because of their overall low number per brain and their exclusive occurrence in capillaries. Finally, the dimension of those accumulated erythrocytes in control animals was much more restricted in comparison with the erythrocyte accumulation in SHRSP. In contrast, the number of SHRSP that contain accumulated erythrocytes in their brain vessels significantly increased with age (Figure 2A). Moreover, the overall extent of vessels with accumulated erythrocytes per brain in older SHRSP increased dramatically, so that virtually all brain regions became affected.

In older SHRSP (older than 28 weeks), erythrocyte accumulations occurred in both capillaries and arteriolar segments, whereas the few accumulated erythrocytes occasionally found in control rats were depicted only in capillaries. Figure 2C illustrates the minimal and maximal diameter of small vessels containing accumulated erythrocytes.

Interestingly, quantification revealed that in the basal ganglia, the diameter of the affected small vessels significantly increased with age of SHRSP (Figure 2C). However, this does not apply to the other brain regions, where the diameter of the vessels with accumulated erythrocytes did not change significantly with age. Moreover, as a general phenomenon, we frequently found brain regions, where erythrocyte accumulations are located in arteriolar segments, but the surrounding capillaries are free of them (Figures 1E and 1F).

Some of the older SHRSP contained brain vessels, where erythrocytes accumulated nearby or within node-like constrictions (Figure 1E). Higher magnifications sometimes revealed single erythrocytes migrating throughout the vessel wall; a process we refer to as diapedesis (Figure 1C′, white arrow head).

Leakage of the Blood–Brain Barrier

We determined the occurrence of IgG deposits in the wall of small vessels in the hippocampus, the basal ganglia, the cortex, and the corpus callosum in SHRSP as a marker for possible BBB leakage (Figure 3). Spontaneously hypertensive stroke-prone rats at the age of 18 weeks were the youngest animals we investigated, which contained IgG deposits in the walls of small vessels. Quantification revealed a significantly increasing extent of BBB disturbances in older animals (Figure 3C). That was the case for all brain regions.

Colabeling with laminin revealed that IgG seems to be deposited between the endothelium and the basal membrane (Figures 3E and 3F). In certain vessels, higher magnification also showed leakage of IgG and

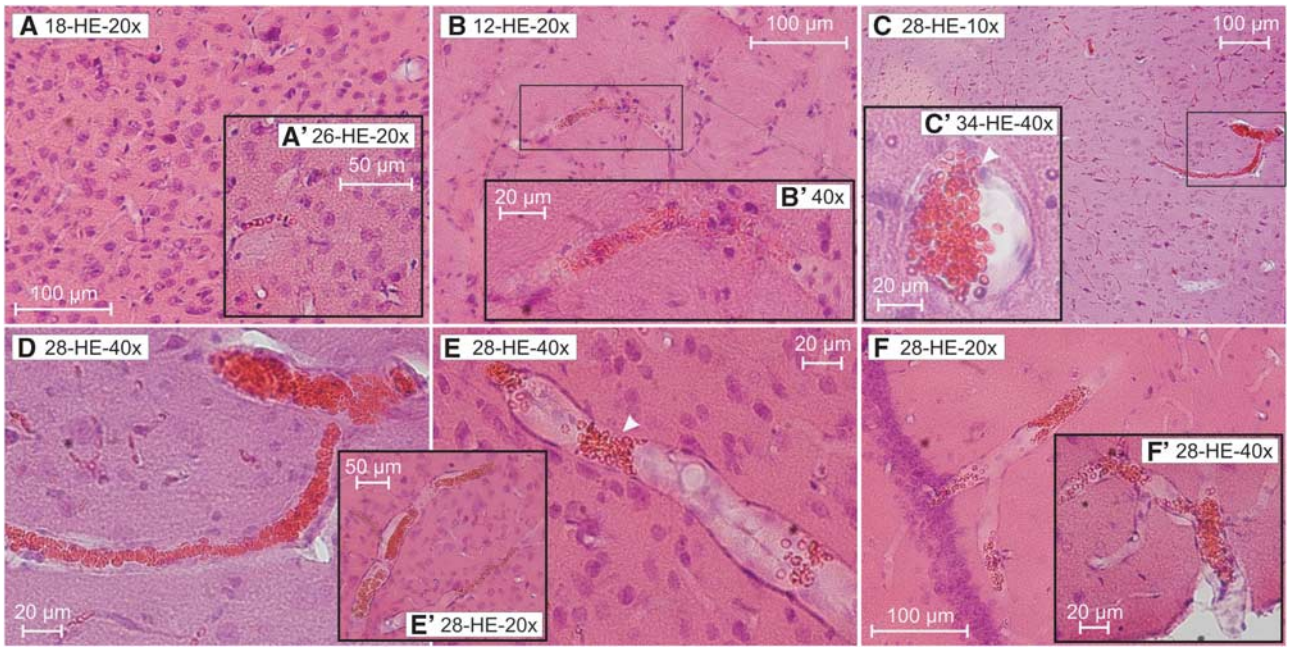

Figure 1 Accumulations of erythrocytes in SHRSP with different ages. Accumulations of erythrocytes in small vessels of the basal ganglia (**B**, **B′**), the cortex (**C**, **D**, **E**, **E′**), and its adjacent meningeal arterioles (**F′**), as well as the hippocampus (**C′**, **F**) occurred in all age groups of the SHRSP (panels **B** and **B′**: 12 weeks old, panels **C**, **D** to **F′**: 28 weeks old, panel **C′**: 34 weeks old). Interestingly, there were brain regions found with accumulating erythrocytes located in arteriolar segments, but the surrounding capillaries were free of them (**E**, **F**). Moreover, single erythrocytes migrate throughout the vascular wall (panel **C′**, white arrow head). In arterioles, erythrocytes often accumulate within segmental vascular node-like constrictions (panel **E**, white arrow head). In comparison, there are no (**A**) or hardly detectable (**A′**) erythrocyte accumulations in the cortex of control animals (panel **A**: 18 weeks old, panel **A′**: 26 weeks old). HE staining. Panel **D** is a higher magnification of panel **C**. HE, Hematoxylin–Eosin; SHRSP, spontaneously hypertensive stroke-prone rat.

therefore plasma into the parenchyma (Figure 3G). Furthermore, Figure 3H illustrates a thrombus in SHRSP with infarcted tissue. Both IgG and laminin appear around the vessel in a disorganized pattern, suggesting vessel wall rupture and therefore bleeding, which had occurred before vessel occlusion.

Microbleeds

In addition to intraluminal accumulations of erythrocytes, we detected extraluminal fresh microbleeds (Figure 4) when animals reached an age of ~32 weeks. These bleedings were characterized by numerous grouped erythrocytes leaking from the small vessels into the parenchyma of the basal ganglia, cortical regions, the hippocampus, and the corpus callosum. We did not detect any microbleeds in control animals. Both the overall number of microbleeds per animal and the percentage of animals with microbleeds in their brain significantly increased with age (Figure 2B).

Vessel Occlusion and Tissue Infarction

Only 5 of all investigated animals (9.8%) exhibited cerebral infarctions (Figures 5C and 6C to 6E), characterized by a salient spongy and cystic tissue destruction. Typically, those infarct regions contain vessels with arteriolar occlusions (Figures 4D and 7D, asterisk). The age of these 5 animals with cerebral infarctions ranged between 32 and 42 weeks (2 animals 32 weeks, 1×36, 1×40, and 1×42 weeks).

Imaging

At the age of 32 weeks, we detected T2 hyperintensive lesions in 2 of the 15 investigated animals (Figures 5A and 5D). The remaining 13 animals displayed no T2 peculiarities. Macroangiopathy was excluded by Time of Flight Angiography in all investigated animals.

Shortly after MRI, these two animals with T2 hyperintensities were scanned using 201-TI-DDC SPECT (Figures 5B and 5E). In those T2 positive regions, the uptake of 201-TI was reduced. The corresponding histology showed infarcted tissue (Figure 5C); one of those two animals additionally exhibited microthromboses, in the other animal, we detected microbleeds (Figure 5F).

One 42-week-old SHRSP with a progressive loss in body weight of 38 g within a time span of 4 weeks simultaneously underwent 201-TI-DDC and 99m-Tc-HMPAO SPECT. The uptake of both tracers was

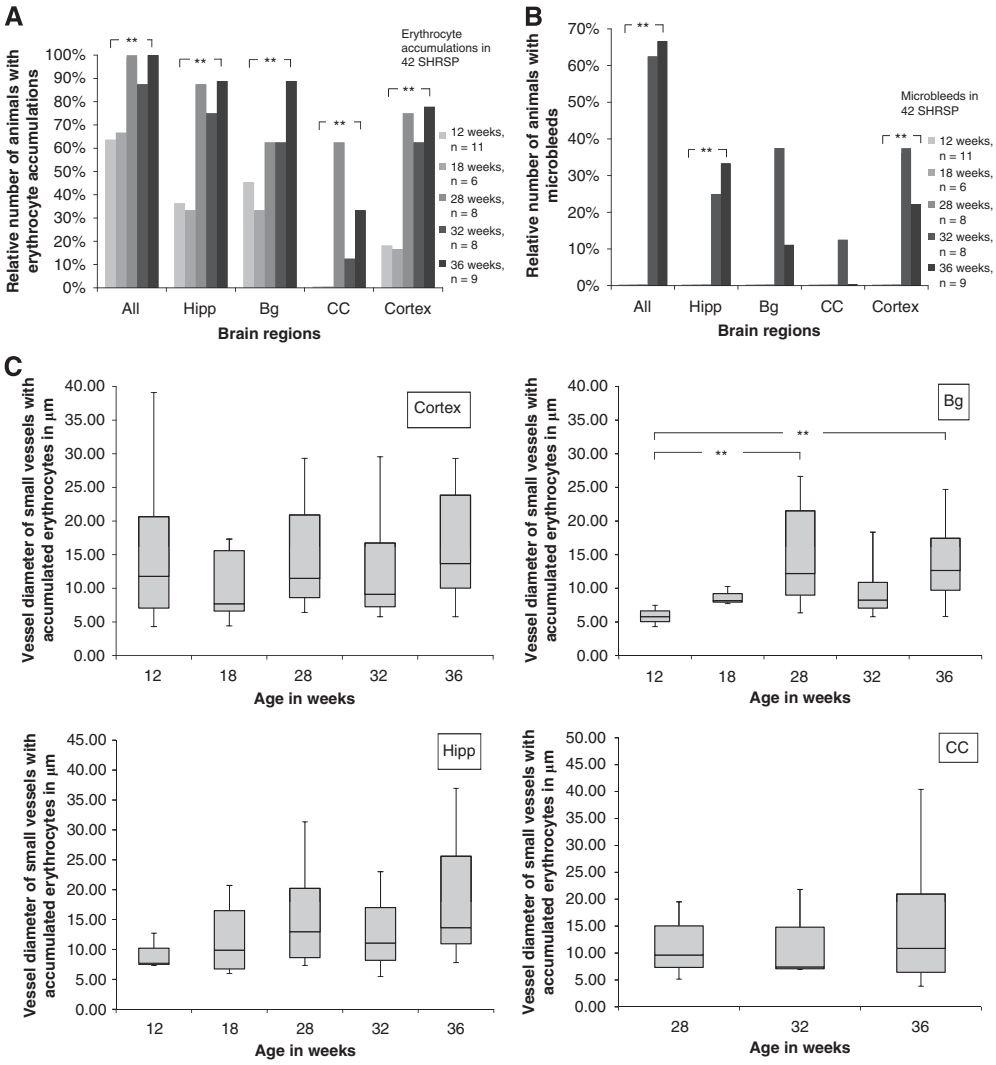

Figure 2 (**A**, **B**) Relative number of SHRSP with accumulations of erythrocytes and microbleeds in different brain regions and at different ages. Relative number of exemplary SHRSP ($n = 42$) with accumulated erythrocytes (panel **A**) and microbleeds (panel **B**). We detected erythrocyte accumulations and microbleeds separately in the hippocampus (Hipp), the basal ganglia (Bg), the corpus callosum (CC), and in the cortex at different stages of age. The number of animals with accumulated erythrocytes and microbleeds in any of the examined brain regions is also given (All). The significant increase of the relative number of SHRSP showing erythrocyte accumulations (panel **A**, all $P = 0.001$, Hipp $P = 0.002$, Bg $P = 0.05$, CC $P = 0.01$, cortex $P = 0.0001$) and microbleeds (panel **B**, all $P = 0.00008$, Hipp $P = 0.012$, cortex $P = 0.022$, Bg $P = 0.055$, CC $P = 0.65$) with the increasing age of that group must be noted. $^{**}P \leq 0.05$. n is the particular total number of investigated animals. (**C**) Luminal diameter of small vessels with accumulated erythrocytes in different brain regions of SHRSP at different ages. Box whiskers plot. We determined the luminal diameters of small vessels with accumulating erythrocytes in different brain regions (Bg, Hipp, CC) at different ages of SHRSP. The median diameter (black bar), the 25th and the 75th percentile (gray box) of the diameter, and the range between the minimal and the maximal diameter (whiskers) of the small vessels are given in μm. In the basal ganglia, the diameter of the affected small vessels significantly increased with the age of SHRSP ($P = 0.003$). In the remaining brain regions, the diameter of the vessels with accumulated erythrocytes did not change significantly with the age of the SHRSP group (cortex $P = 0.149$, Hipp $P = 0.135$, CC $P = 0.765$). $^{**}P \leq 0.05$. SHRSP, spontaneously hypertensive stroke-prone rat.

reduced in the same brain regions (Figures 6A and 6B). In the corresponding histology, we detected tissue infarctions and microbleeds (Figures 6C to 6E).

Cerebral Amyloid Angiopathy

Cerebral Amyloid Angiopathy could not be detected by polarized light after Congo Red staining in any of the disease stages.

Discussion

In this study, we investigated the spontaneous development of the vascular pathology in SHRSP. Spontaneously hypertensive stroke-prone rats were bred from spontaneously hypertensive (SH) rats under the criteria of cerebral infarct development. With increasing age, SHRSP develop a number of risk factors including hypertension, insulin resistance, hyperinsulinemia, hypertriglyceridemia,

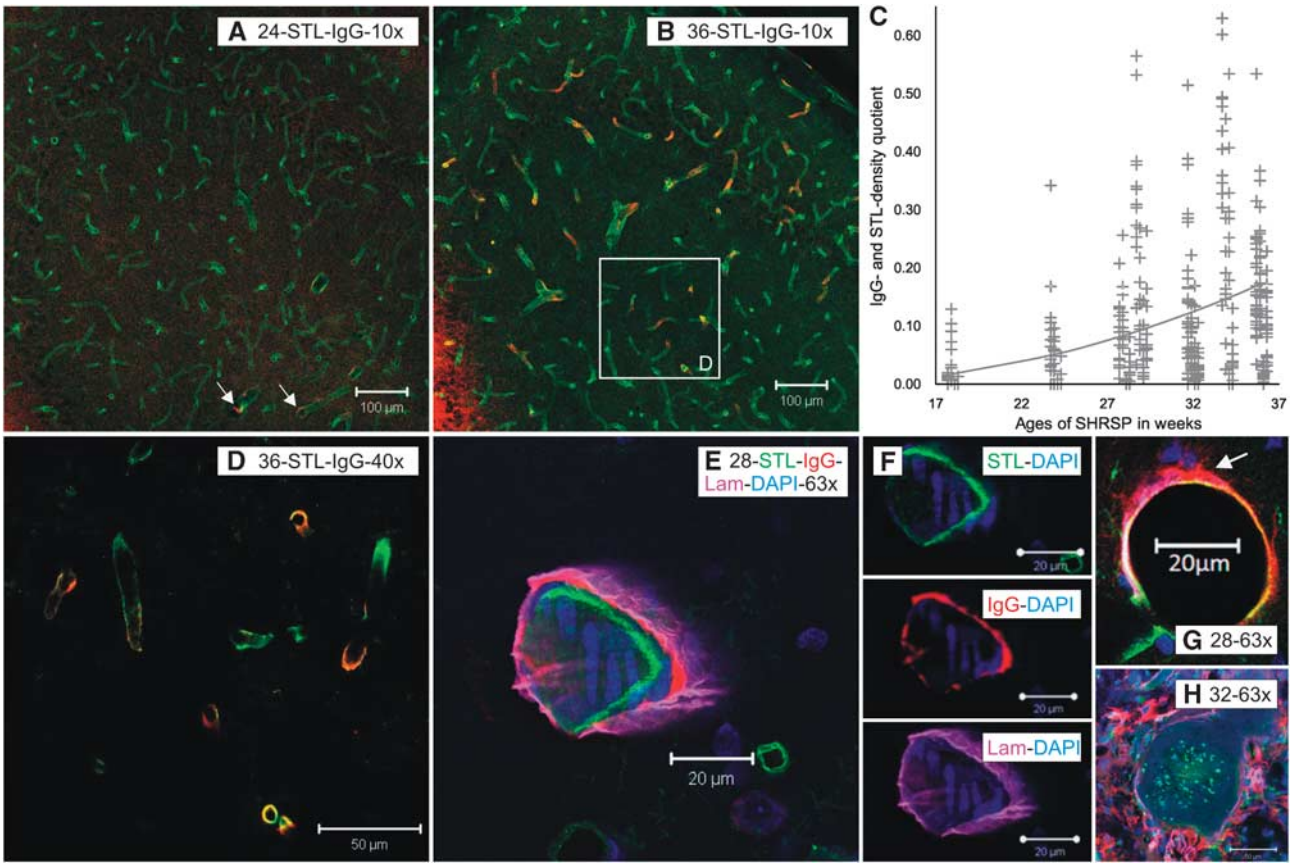

Figure 3 STL-, laminin-, and IgG-immunoreactive vessels and ratio of the densities of IgG- and STL-positive vessels in SHRSP with different ages. STL (green)- and IgG (red)-positive vessels are shown in the hippocampus of 24-week-old (**A**) and 36-week-old (**B**, **D**, and **E**) SHRSP. The small number of IgG-immunoreactive vessels in the younger animal (panel **A**, 24 weeks, white arrows) and its increase with age (panel **B**, 36 weeks) must be noted. Panel **D** shows the histologic magnification in different *z*-planes of the white rectangle in panel **B**. In panel **C**, the ratio of the densities of IgG- and STL-positive vessels in SHRSP is plotted over the different ages of the 9 investigated animals. The result of every counting box is given by a marker in the plot. The resulting parabolic regression function for all regions is depicted by the line. The significant increase of the ratio over the time in all of the investigated regions ($P = 0.008$) showing an increasing blood–brain barrier disturbance in older SHRSP. In panels **E** to **G**, confocal analysis illustrates that IgG (red) is deposited most likely between the endothelium (STL in green) and the basal membrane (Lam-laminin in pink). However, in certain vessel IgG, i.e., plasma is also entering the parenchyma (panel **G**, white arrow). A thrombus is shown in panel **H**; both IgG and laminin patterns illustrate the rupture of the vessel wall, suggesting that a bleeding had preceded vessel occlusion. SHRSP, spontaneously hypertensive stroke-prone rat; STL, solanum tuberosum lectin.

hypercholesterolemia, and nephropathy. Thus, SHRSP represent the same multimorbidity as it is found in many stroke patients and in patients with vascular dementia. Hence, these rats are completely different from many used animals in experimental models. Therefore, we believe that important pathophysiological steps not equated but common to human CSVD can be observed in the animal model of SHRSP. This model especially allows the histologic description of the initial pathologic steps, which is rather impossible under clinical conditions.

Our histologic investigations of SHRSP at different stages of age revealed a progression of small vessel changes in several steps. Accumulations of erythrocytes parsimoniously interpreted as stases were thereby the first pathologic phenomenon we were able to capture. These stases can be described as aggregations of erythrocytes in small cerebral vessels to a greater or lesser extent (Figure 1). Already at the age of 12 weeks, we found accumulated erythrocytes in ~60% of all investigated SHRSP. However, both the dimension of single erythrocyte accumulations and the number of erythrocyte accumulations per brain were rather small in those animals aged 12 weeks (Figures 1B and 2A).

However, reaching an age of 28 weeks, all investigated SHRSP contained accumulated erythrocytes, whereby the number of erythrocyte accumulations per brain had increased dramatically, so that in fact every brain region was affected by those accumulated erythrocytes. Moreover, the dimension of single erythrocyte accumulations increased considerably (Figures 1C to 1F). Interestingly, we occasionally also found accumulated erythrocytes in healthy control animals.

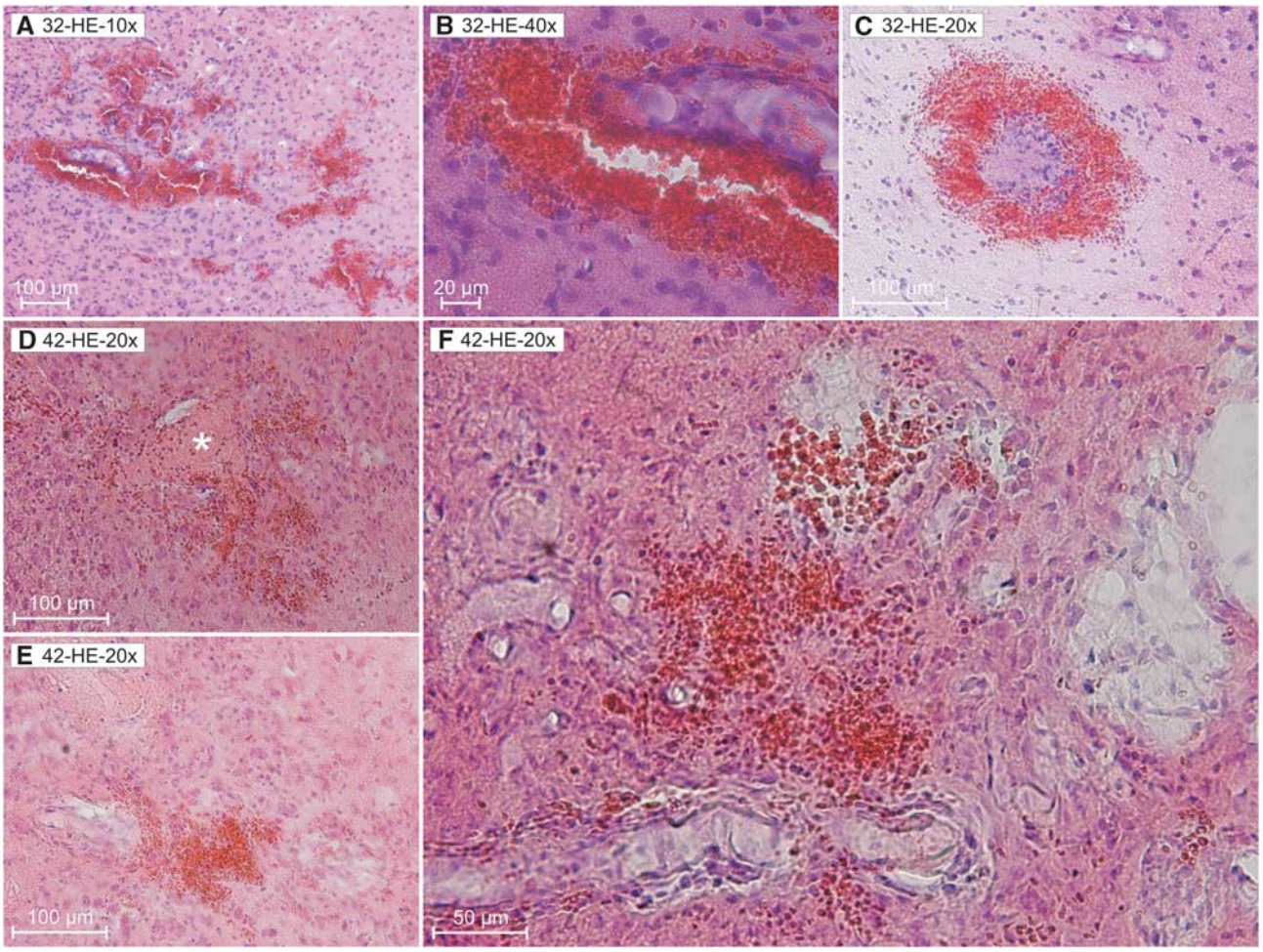

Figure 4 Microbleeds in SHRSP at different stages of age. From the 32nd week on, we detected numerous microbleeds in the brain tissue of SHRSP (**A** to **C** 32 weeks of age). Panels **D** to **F** illustrates the infarct region of a 42-week-old SHRSP. Infarcted tissue contains spongy and cystic tissue destructions with fresh and older microbleeds and also occluded vessels (panel **D**, asterisk). Panel **F** corresponds to **Figure 6D** rotated 90° counterclockwise HE staining. HE, Hematoxylin–Eosin; SHRSP, spontaneously hypertensive stroke-prone rat.

For this purpose, we examined Wistar rats aged between 12 and 65 weeks. In ~25% of all these rats, we depicted single erythrocyte accumulations (Figure 1A′). However, the dimension of those accumulated erythrocytes was much smaller than in SHRSP. Therefore, we conclude that erythrocyte accumulations represent a phenomenon, sporadically occurring in healthy rats, too. Whether this symptom becomes more frequent in older control animals might be only determined in a great population of aged healthy rats.

Strikingly, the rare erythrocyte accumulations with always small dimensions in control rats were only found in capillaries. In contrast, SHRSP aged ⩾28 weeks incorporate accumulated erythrocytes frequently in cerebral arterioles, i.e., in small vessels with a luminal diameter of at least 22 μm. We predominantly observed that progressive 'affection' of arterioles in the SHRSP' basal ganglia (Figure 2C), one of the early affected structures in human CSVD (Grinberg and Thal, 2010). Moreover, in SHRSP, we detected brain regions, in which arterioles were affected by erythrocyte accumulations, whereas neighboring capillaries were free of those accumulating erythrocytes (Figures 1E and 1F). As outlined in the 'Materials and methods' section, we referred to capillaries when the diameter was smaller than 22 μm. If the small vessel emerges directly from an arteriole, it can be defined as a capillary. However, it has to be mentioned that in all other cases, we are not able to discriminate between capillaries and venules. Interestingly, in many cases, it became obvious that accumulating erythrocytes were located in the direct proximity of node-like vessel constrictions. We assume that these vessel constrictions are an important milestone in the pathologic cascade of the vascular pathology in SHRSP.

The dramatic increase in both the number and the size of erythrocyte accumulations per animal in 28-week-old SHRSP and the location of accumulated erythrocytes in arterioles with node-like constrictions make it highly supposable that erythrocyte

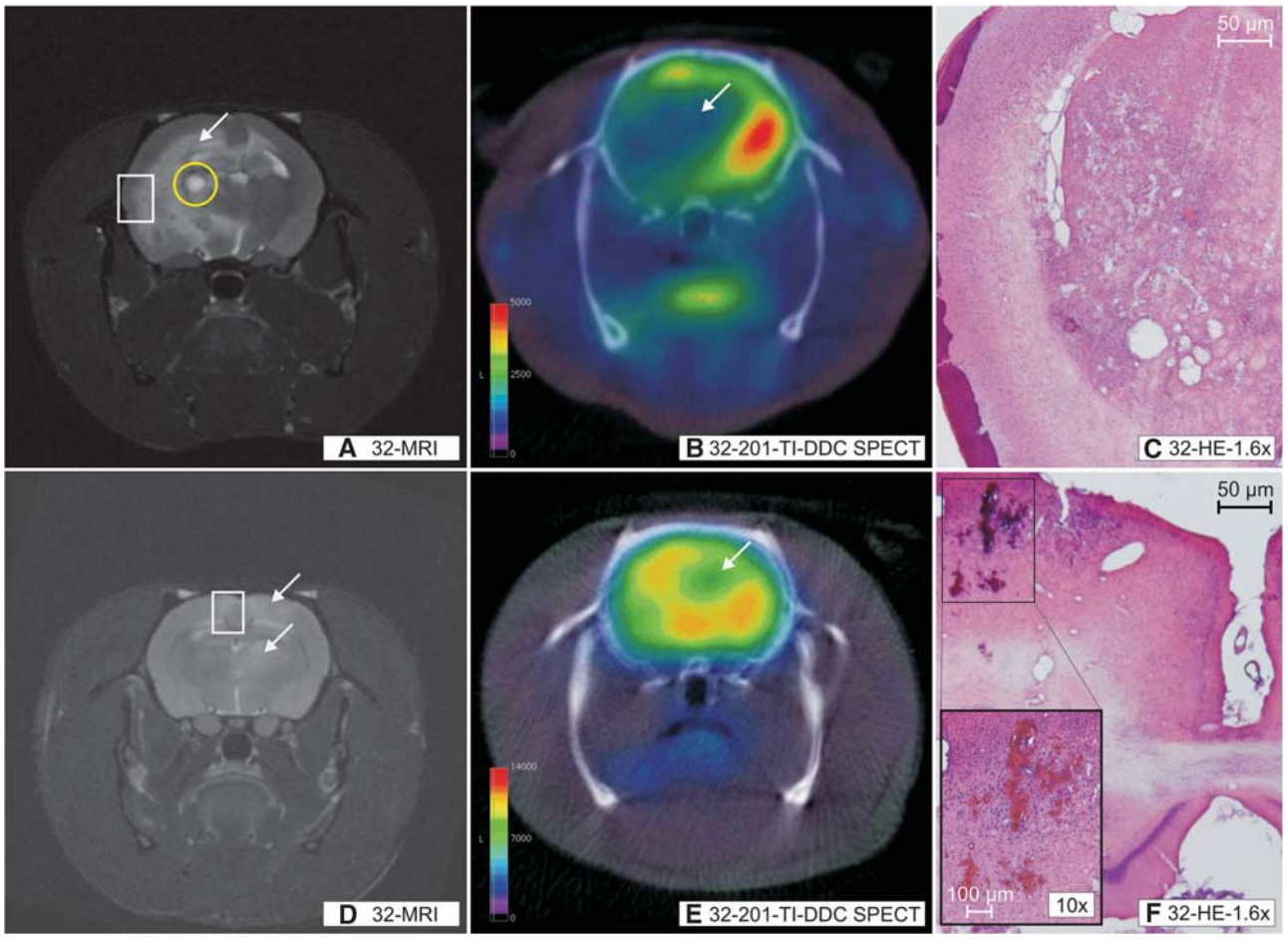

Figure 5 MRI, 201-TI-DDC SPECT and histology performed in the same animals. T2 sequences (**A**, **D**) and 201-TI-DDC SPECT (**B**, **E**) with coronal slice orientation performed in the same animal: animal 4 (32 weeks, upper row) and animal 16 (32 weeks, lower row). It must be noted that those regions being T2 hyperintensive in MRI (panels **A** and **D**, white arrows) show a reduction of 201-TI-DDC uptake (panels **B** and **E**, white arrows). In the corresponding histology, infarcted tissue (**C**; HE staining) and microbleeds (**F**, HE staining; panel **F**: figure in the left lower corner HE staining) were detected. Panels **C** and **F** correspond to the white rectangle in panels **A** and **D**. The small subacute bleeding in the basal ganglia of animal 4 (panel **A**, yellow circle) must be noted. HE, Hematoxylin–Eosin; MRI, Magnetic Resonance Imaging; SHRSP, spontaneously hypertensive stroke-prone rat; SPECT, Single Photon Emission Computed Tomography; 201-TI-DDC, 201-Thallium-Diethyldithiocarbamate.

accumulations develop as an initial step owing to so far undefined changes in small vessels rather to be the result of an insufficient transcardial perfusion. Indeed, the definitive (and very difficult to render) evidence for the existence of detected erythrocyte accumulations as stases in living animals can be exclusively provided by *in vivo* imaging techniques.

Whether smooth muscle cell contractions of the tunica media cause these constrictions and why they occur, remains unclear. Several alterations have been described in mesenteric arteries of SHRSP, e.g., reduced density in the media with concurrent increased volume and reduced arterial lumen (Arribas *et al*, 1997). Furthermore, the authors found indications for a reduced number of endothelial cells. It is likely that similar phenomena occur in cerebral arteries.

Under conditions of experimental ischemia Yemisci *et al* (2009) also observed accumulations of erythrocytes. The authors argue that oxidative stress after reperfusion damages pericytes and induces abnormal contractions of those cells. Contrary to our results, Yemisci *et al* (2009) describe the accumulated erythrocytes to be present only in capillaries. Moreover, Henning *et al* (2010) depicted accumulating erythrocytes in small vessels of old female SHRSP. These authors assume that the accumulation of erythrocytes is the consequence of a vessel compression caused by an adjacent tissue edema after cerebral infarctions. Contrary to their conclusions, our data show that those accumulated erythrocytes are not caused by tissue infarctions, but instead represent the early stage of the vascular pathology in SHRSP.

Higher magnifications of erythrocyte accumulations show that single erythrocytes escape from the lumen of the vessel (Figure 1C′). It remains unclear whether these diapedeses indicate subsequent microbleeds.

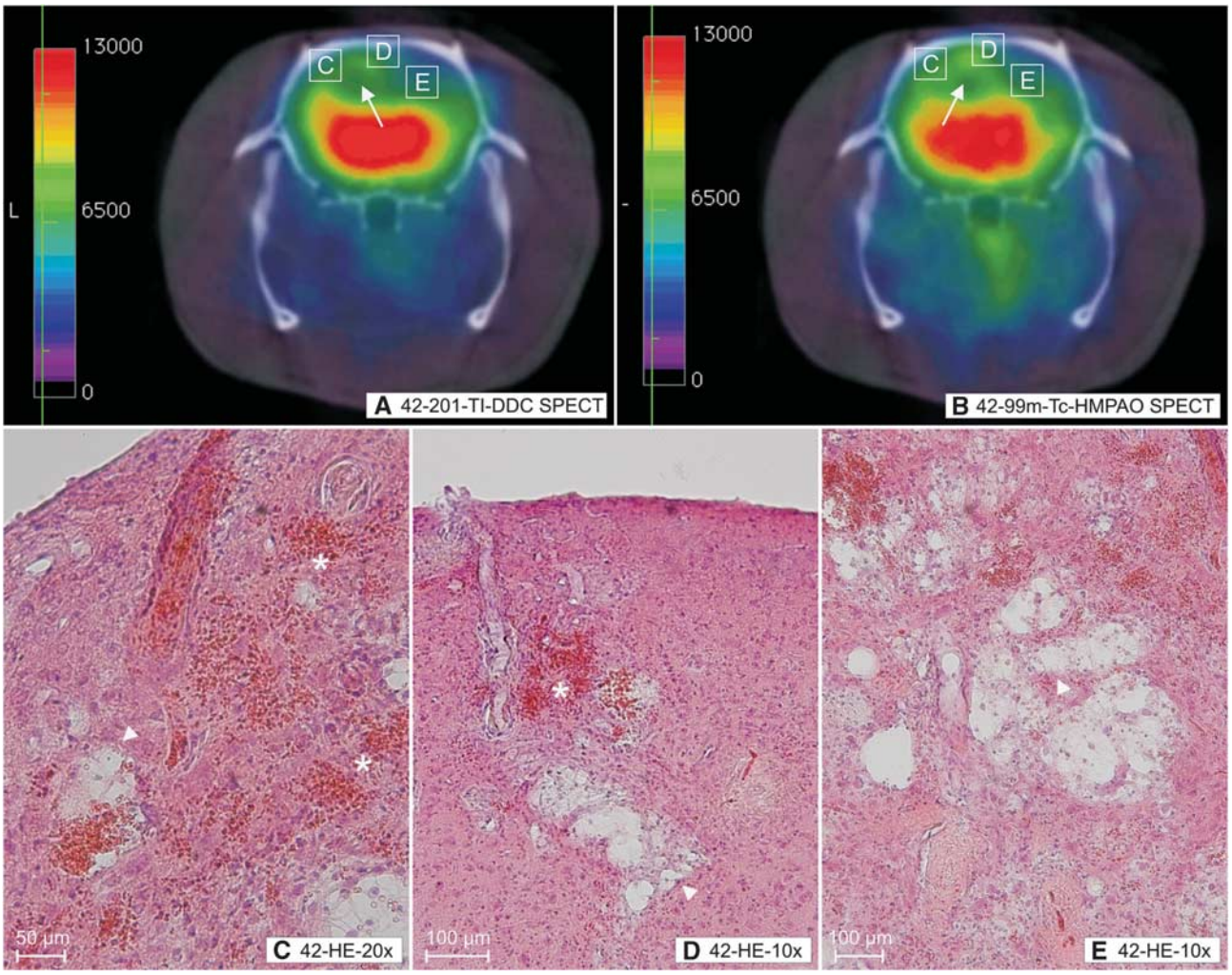

Figure 6 201-TI-DDC SPECT, 99m-Tc-HMPAO SPECT, and histology performed in the same animal. (**A**) 201-TI-DDC and (**B**) 99m-Tc-HMPAO SPECT with coronal slice orientation performed in the same animal (animal 202, 42 weeks). It must be noted that those green pseudo-colored regions in the cortex and the white matter of both hemispheres (panels **A** and **B** white arrows) depict a reduction of 201-TI-DDC (panel **A**) and 99m-Tc (panel **B**) uptake. In the corresponding histology, we detected infarctions with consequent spongy and cystic tissue destructions (**C** to **E**, white arrow heads) and microbleeds (panels **C** and **D** asterisks) in those regions with reduced tracer uptakes. Panels **C** to **E** show the histologic magnification of the white rectangles in panels **A** and **B**. Panel **D** corresponds to **Figure 4F** rotated 90° clockwise. HE staining. HE, Hematoxylin–Eosin; MRI, Magnetic Resonance Imaging; 99m-Tc-HMPAO, 99m-Technetium-HMPAO; SHRSP, spontaneously hypertensive stroke-prone rat; SPECT, Single Photon Emission Computed Tomography; 201-TI-DDC, 201-Thallium-Diethyldithiocarbamate.

Furthermore, we detected a leakage of IgG into the wall of the small vessels. Those changes represent BBB disturbances (Grinberg and Thal, 2010), occurring some weeks after we depicted accumulated erythrocytes and are highly concentrated in older SHRSP. Endothelial disruption with subsequent BBB breakdown has been described to be the primary event preceding microthromboses and lacunar infarcts, as well as microbleeds and white matter cysts (Bailey *et al*, 2009). Our data indicate that the initial BBB disturbances are restricted to a leakage of IgG into the vessel wall and are not associated with a vessel wall disruption. Our colabeling with laminin suggests that IgG is deposited between the endothelium and the basal membrane. However, it also revealed that in certain blood vessels, IgG and therefore plasma already entered the parenchyma at a stage in which the vessel wall looks morphologically still intact (Figure 3). Interestingly, both initial changes—the accumulation of erythrocytes and the early plasma protein leakage into the vessel wall—are not associated with arteriolar occlusions. Rather, subsequent microbleeds, tissue infarctions with occluded vessels, vasogenic edema, and white matter cysts occur for the first time several weeks after the initial BBB disturbances have been detected.

We first detected microbleeds in SHRSP at the age of ~32 weeks. These microbleeds were distributed irregularly in all brain regions and obviously developed at different time points. Interestingly, brain

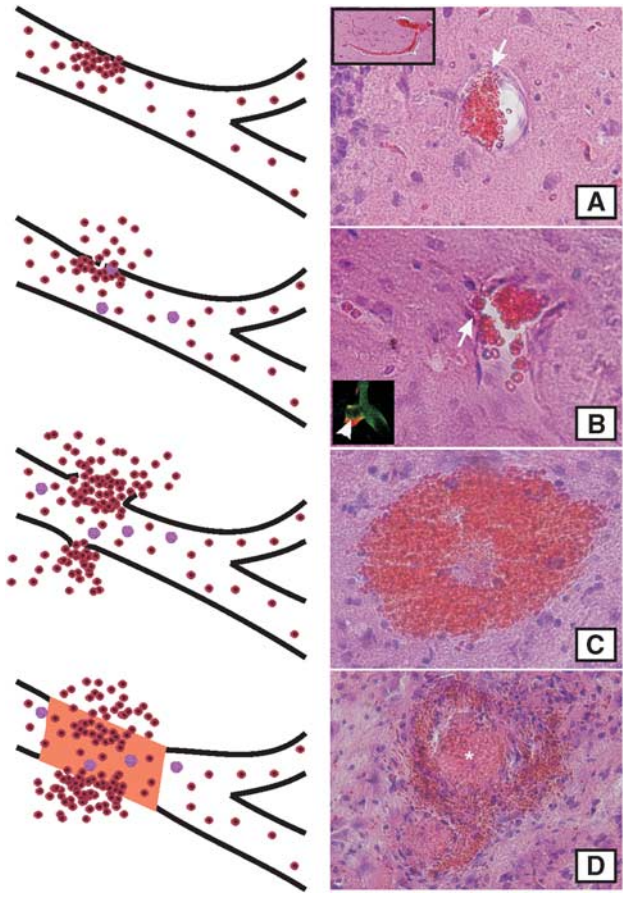

Figure 7 Stages of the vascular pathology in SHRSP. Accumulations of erythrocytes in capillaries and arterioles display the quite common initial step of the vascular pathology in SHRSP (**A**, step one). Some weeks later, disturbances of the blood–brain barrier (BBB) (step two) were detected. BBB disturbances are illustrated by a leakage of IgG deposits into the vascular wall (**B**, white arrow head in the rectangle in the left lower corner) and by the migration of single erythrocytes throughout the small vessel wall (panels **A** and **B**, white arrows). Several weeks after the BBB leakage, microbleeds occurred (**C**, step three) immediately followed by (reactive) microthromboses (**D**, asterisk, step four). Microbleeds and vessel occlusions cause cystic and spongy tissue infarctions (shown in **Figures 4** to **6**). SHRSP, spontaneously hypertensive stroke-prone rat.

regions containing microbleeds were almost free of erythrocyte accumulations. Although not provable by our data, it is conceivable that those vessels with accumulated erythrocytes at earlier age are conspicuously fragile and give rise to microbleeds by vessel wall disruption at older age. This is supported by node-like constrictions of vessels described above and often found to be associated with accumulating erythrocytes. The ultimate cause for this fragility remains open, but arterial hypertension associated endothelial proliferation with splitting of the lamina elastica interna, plasma protein leakage, and fibrinoid necrosis (Grinberg and Thal, 2010), as well as additional age-associated changes of the vessel wall might force this fragility until the rupture of small vessels and consequent bleedings (Rizzoni and Agabiti, 2006).

As expected, there were no signs of CAA in our SHRSP; massive depositions of Aβ do not occur in vessel walls. Thus, CAA can be excluded as a reason for bleedings because it is described in humans (Grinberg and Thal, 2010).

Rats with number T5 and T16 are examples of SHRSP containing a high number of microbleeds (Figures 4A to 4C) without extended tissue necrosis/infarctions. Tissue infarctions obviously represent the final stage of the SHRSP' vascular pathology and might develop shortly after the occurrence of microbleeds (e.g., rat number T202, Figure 6). Thus, fairly big areas with infarctions contain fresh and older microbleeds, as well as ruptured blood vessels with subsequent occlusions (Figures 4D to 4F).

These tissue infarctions were detectable by T2 hyperintensities in MRI (Figures 5A and 5D). The associated (vasogenic) tissue edema caused a further compression of still intact vessels lying in the periphery of the infarct area. This leads to hypoperfusion of extended brain regions by an additional reduction of CBF (Henning *et al*, 2010), and potassium uptake as revealed by 99m-Tc-HMPAO and 201-Tl-DDC SPECT (Figures 5 and 6). Our SPECT study is a pilot study aiming to investigate whether or how pathologic alterations detectable by MRI or histology correlate with changes in potassium uptake and blood flow. The results of these studies are promising and indicate that SPECT Imaging can be a useful imaging modality in monitoring disease progression or potential therapeutic effects in drug testing in SHRSP.

Interestingly, our data indicate that microbleeds seem to precede microthromboses rather than follow them. Thus, our results might provide an explanation why microbleeds have been described to be independent predictors of recurrent ischemic stroke in humans (Thijs *et al*, 2010).

Taking all data together, we described the pathogenesis of the vascular pathology in SHRSP as follows: By reasons, we do not know yet, aggregations of erythrocytes develop in arterioles and capillaries (Figure 7A). Constrictions of the vessel wall often found in direct vicinity of accumulating erythrocytes let us presume that autoregulatory changes of the vessel tonus might be involved here. Depositions of plasma proteins (IgG) in the vessel wall (Figures 3 and 7B) together with other factors not investigated in this study (severe arterial hypertension with systolic values of at least 200 mm Hg since an age of $\sim$10 weeks (Yamori *et al*, 1976) and diabetes) induce permanent injuries of the vessel wall. The consequence is an increased permeability of the BBB which possibly can be recognized by diapedeses of single erythrocytes (Figures 1C′ and 7B). Finally, the integrity of blood vessels becomes damaged in a degree that multitude microbleeds occur at different time points after rupture of the

vessel walls (Figures 4A to 4C and 7C), resulting in hemorrhagic microinfarctions (Figures 4D to 4F).

The cumulative appearance of microinfarcts in one brain region can induce expanded tissue necrosis (Figure 5A) otherwise typical for occlusions of bigger brain vessels (macroangiopathy) or cerebral lesions of SHRSP fed a salt loaded diet with 1% NaCl added to their drinking water (Guerrini *et al*, 2002). The development of (vasogenic) edema illustrated by T2 sequences in MRI (Figures 5A and 5D) further decreases CBF (Figure 6B). Finally, occlusions of vessels (Figures 4D and 7D) develop as a reaction to microbleeds and can therefore be observed in infarct regions together with fresh and old microbleeds.

We emphasize that in contrast to other authors, we did not apply a diet with 1% salt in drinking water (Lee *et al*, 2007; Gelosa *et al*, 2010). Therefore, in animals fed a salt-loaded diet, tissue infarctions occur in 80% of 30-week-old male SHRSP (Yamori and Horie, 1977; Tagami *et al*, 1987). On the contrary, the average onset for corresponding symptoms in SHRSP fed a standard diet without supplemental salt is 9 months (male rats) and 1.2 years (female rats) (Henning *et al*, 2010). Obviously, the abnormal uptake of salt causes an accelerated damage of vessel walls (SHRSP develop cerebral lesions after 42 ± 3 days after starting a salt enhanced diet (Guerrini *et al*, 2002)) and a fast development of hypertension (the systolic blood pressure increases about at least 40 mm Hg during those 42 ± 3 days (Henning *et al*, 2010)). Nevertheless, because there is a lack of longitudinal studies combining imaging and blood pressure data, it is still a matter of debate whether there is any definite association between an aggravation of arterial hypertension and the development of cerebral lesions in SHRSP (Henning *et al*, 2010). However, we believe that omitting a salt diet is one of the major advantages of our study in such a way that our animals might represent the real complexity of the natural progression of CSVD. The price for that is a more inhomogeneous temporal course of the described pathology.

Irrespective from the exact time point of the onset of cerebral lesions in a single animal, the appearance of erythrocyte aggregations seems to be the initial step of the vascular pathology in SHRSP.

Therefore, we believe the animal model of SHRSP to provide important insights for the understanding of human CSVD. Thus, we assume that a certain cohort of patients with CSVD may have a cumulative appearance of independent microbleeds occurring at different time points. It has to be elucidated whether accumulations of erythrocytes described here in the model of SHRSP also stand at the beginning of the pathologic cascade of certain patients with CSVD. The diagnosis of these erythrocyte aggregations or alternatively the definition of their diagnostic correlates (e.g., serum parameters) would allow an efficient prevention at a time point, when microbleeds and vessel occlusions have not been developed yet. By this means, the progress of human CSVD could be stopped at a stage before severe neurologic symptoms and cognitive deficits occur.

Acknowledgements

The authors thank Ines Heinemann, Deutsches Zentrum für Neurodegenerative Erkrankungen, Magdeburg, for the assistance by performing the imaging. The authors also thank Christian Mawrin, Institute for Neuropathology, Otto-von-Guericke University, Magdeburg, for histologic advice and for analysis of those slices stained with Congo Red.

Disclosure/conflict of interest

The authors declare no conflict of interest.

References

Amarenco P, Bogousslavsky J, Caplan LR, Donnan GA, Hennerici MG (2009) Classification of stroke subtypes. *Cerebrovasc Dis* 27:493–501

Arribas SM, Hillier C, Gonzalez C, McGrory S, Dominiczak AF, McGrath JC (1997) Cellular aspects of vascular remodeling in hypertension revealed by confocal microscopy. *Hypertension* 30:1455–64

Bailey EL, McCulloch J, Sudlow C, Wardlaw JM (2009) Potential animal models of lacunar stroke: a systematic review. *Stroke* 40:e451–8

de Bruine JF, van Royen EA, Vyth A, de Jong JM, van der Schoot JB (1985) Thallium-201 diethyldithiocarbamate: an alternative to iodine-123 N-isopropyl-p-iodoamphetamine. *J Nucl Med* 26:925–30

Fotuhi M, Hachinski V, Whitehouse PJ (2009) Changing perspectives regarding late-life dementia. *Nat Rev Neurol* 5:649–58

Gelosa P, Ballerio R, Banfi C, Nobili E, Gianella A, Pignieri A, Brioschi M, Guerrini U, Castiglioni L, Blanc-Guillemaud V, Lerond L, Tremoli E, Sironi L (2010) Terutroban, a TP receptor antagonist, increases survival in stroke-prone rats by preventing systemic inflammation and endothelial dysfunction. Comparison with Aspirin and Rosuvastatin. *J Pharmacol Exp Ther* 334:199–205

Goldschmidt J, Wanger T, Engelhorn A, Friedrich H, Happel M, Ilango A, Engelmann M, Stuermer IW, Ohl FW, Scheich H (2010) High-resolution mapping of neuronal activity using the lipophilic thallium chelate complex TlDDC: protocol and validation of the method. *Neuroimage* 49:303–15

Gouw AA, Seewann A, van der Flier WM, Barkhof F, Rozemuller AM, Scheltens P, Geurts JJ (2010) Heterogeneity of small vessel disease: a systematic review of MRI and histopathology correlations. *J Neurol Neurosurg Psychiatry* 82:126–35

Grinberg LT, Thal DR (2010) Vascular pathology in the aged human brain. *Acta Neuropathol* 119:277–90

Guerrini U, Sironi L, Tremoli E, Cimino M, Pollo B, Calvio AM, Paoletti R, Asdente M (2002) New insights into brain damage in stroke-prone rats: a nuclear magnetic imaging study. *Stroke* 33:825–30

Hainsworth AH, Markus HS (2008) Do *in vivo* experimental models reflect human cerebral small vessel disease? A systematic review. *J Cereb Blood Flow Metab* 28: 1877–91

Hennig J, Nauerth A, Friedburg H (1986) RARE imaging: a fast imaging method for clinical MR. *Magn Reson Med* 3:823–33

Henning EC, Warach S, Spatz M (2010) Hypertension-induced vascular remodeling contributes to reduced cerebral perfusion and the development of spontaneous stroke in aged SHRSP rats. *J Cereb Blood Flow Metab* 30:827–36

Lee JM, Zhai G, Liu Q, Gonzales ER, Yin K, Yan P, Hsu CY, Vo KD, Lin W (2007) Vascular permeability precedes spontaneous intracerebral hemorrhage in stroke-prone spontaneously hypertensive rats. *Stroke* 38:3289–91

Ley K, Pries AR, Gaehtgens P (1986) Topological structure of rat mesenteric microvessel networks. *Microvasc Res* 32:315–32

Michalski D, Grosche J, Pelz J, Schneider D, Weise C, Bauer U, Kacza J, Gartner U, Hobohm C, Hartig W (2010) A novel quantification of blood-brain barrier damage and histochemical typing after embolic stroke in rats. *Brain Res* 1359:186–200

Nag S, Manias JL, Stewart DJ (2009) Pathology and new players in the pathogenesis of brain edema. *Acta Neuropathol* 118:197–217

Neirinckx RD, Canning LR, Piper IM, Nowotnik DP, Pickett RD, Holmes RA, Volkert WA, Forster AM, Weisner PS, Marriott JA (1987) Technetium-99m d,l-HM-PAO: a new radiopharmaceutical for SPECT imaging of regional cerebral blood perfusion. *J Nucl Med* 28:191–202

Rizzoni D, Agabiti RE (2006) Small artery remodeling in hypertension and diabetes. *Curr Hypertens Rep* 8: 90–5

Tagami M, Nara Y, Kubota A, Sunaga T, Maezawa H, Fujino H, Yamori Y (1987) Ultrastructural characteristics of occluded perforating arteries in stroke-prone spontaneously hypertensive rats. *Stroke* 18:733–40

Thijs V, Lemmens R, Schoofs C, Gorner A, Van Damme P, Schrooten M, Demaerel P (2010) Microbleeds and the risk of recurrent stroke. *Stroke* 41:2005–9

Van Damme EJ, Barre A, Rouge P, Peumans WJ (2004) Potato lectin: an updated model of a unique chimeric plant protein. *Plant J* 37:34–45

Yamori Y, Horie R (1977) Developmental course of hypertension and regional cerebral blood flow in stroke-prone spontaneously hypertensive rats. *Stroke* 8:456–61

Yamori Y, Horie R, Handa H, Sato M, Fukase M (1976) Pathogenetic similarity of strokes in stroke-prone spontaneously hypertensive rats and humans. *Stroke* 7:46–53

Yang ST, Mayhan WG, Faraci FM, Heistad DD (1991) Mechanisms of impaired endothelium-dependent cerebral vasodilatation in response to bradykinin in hypertensive rats. *Stroke* 22:1177–82

Yemisci M, Gursoy-Ozdemir Y, Vural A, Can A, Topalkara K, Dalkara T (2009) Pericyte contraction induced by oxidative-nitrative stress impairs capillary reflow despite successful opening of an occluded cerebral artery. *Nat Med* 15:1031–7